CO_2-broken Ti-O bonds in TiO_6 octahedron of $CaTiO_3$ for greatly enhanced room-temperature ferromagnetism

Yuqi Ouyang [a #], Bo Gao [a #], Yaozheng Tang [a], Lianyu Li [a] and Qun Xu * [a b]

[a] College of Materials Science and Engineering, Zhengzhou University, Zhengzhou 450052, P.R. China;

[b] Henan Institute of Advanced Technology, Zhengzhou University, Zhengzhou 450052, P.R. China.

E-mail: qunxu@zzu.edu.cn

Table of Contents

1. Supplementary Methods

1.1 Materials.

Commercial $CaTiO_3$ powder is purchased from Sigma Aldrich and can be used without further purification, 99.99% pure CO_2 was provided by Zhengzhou Shuang yang Gas Company as the receiver. All the experimental ethanol was purchased from China Medical Chemical Reagent Co., LTD., and deionized water was prepared with double-distilled water.

1.2 Exfoliation process and preparation of heterostructures.

The SC CO_2 apparatus used for this experiment was composed mainly of a stainless steel autoclave (50 mL) with a heating jacket and a temperature controller. In this study, 60 mg bulk $CaTiO_3$ was dispersed in 30 mL of ethanol/water ($V_{ethanol}$: V_{water} = 1:1) solution and subjected to ultrasonic treatment for 4 hours. The resulting suspension was labeled as ultrasonicated $CaTiO_3$. Meanwhile, the autoclave was heated up to 40℃. Then the ultrasonicated $CaTiO_3$ was immediately transferred into the autoclave, and CO_2 was subsequently charged into the autoclave to the desired pressure (12/14/16 MPa) under stirring. During the exfoliation process, the temperature and pressure of the autoclave were kept constant. After reaction for 4 hours in the condition of SC CO_2, the system was slowly depressurized and the sample was collected. The resulting dispersion was centrifuged at 4500 r.p.m. for 10 minutes to remove the aggregates, and the precipitated supernatant was collected at 10000 r.p.m. for 15 minutes. Finally, the precipitates were dried in the oven at 60 °C.

1.3 Characterization.

Transmission electron microscope (TEM) images were recorded on a FEI Tecnai G2-F20 at an acceleration voltage of 200 kV. The thickness of nanosheets was measured by atomic force microscope (Bruker Dimension Icon). X-ray diffraction (XRD) patterns were collected on a Bruker D8 Focus diffractometer (Bruker AXS, Germany) using Cu Kradiation. X-ray photoelectron spectroscopy (XPS) was performed using Thermo Scientific K-Alpha+ system. Raman measurements were performed using LabRAM HR Evolution with laser wavelength of 830 nm. The

electron paramagnetic resonances were obtained by Electron Paramagnetic Resonance Spectrometer (EMX-9.5/12). The magnetic measurement was carried out with a Physical Property Measurement System (quantum design, PPMS-9) and the magnetic hysteresis loop is observed in the range of -30k Oe < H < 30k Oe at room temperature. K-edge analysis was performed with Si(111) crystal monochromators at the BL11B beamlines at the Shanghai Synchrotron Radiation Facility (SSRF) (Shanghai, China). Before the analysis at the beamline, samples were pressed into thin sheets with 1 cm in diameter and sealed using Kapton tape film. The XAFS spectra were recorded at room temperature using a 4-channel Silicon Drift Detector (SDD) Bruker 5040. Negligible changes in the line-shape and peak position of K-edge XANES spectra were observed between two scans taken for a specific sample. The spectra were processed and analyzed by the software codes Athena.

1.4 Computational Details.

The theoretical calculation based on density functional theory was completed by the VASP software package,[1] and the projector augmented wave (PAW) method[2] was used to describe the ion-electron interaction. Furthermore, Perdew Burke-Ernzerhof (PBE) functional[3] was used to describe the exchange-correlation energy of the simulation system, and DFT-D3[4] was used to improve the calculation accuracy of dispersion force. The cutoff energy of plane wave basis was 500 eV, and the Monkhorst Pack scheme was used to generate k-points with a density of 0.4 per Angstrom for Brillouin zone sampling. The self-consistent field (SCF) calculation was kept within the energy convergence criterion of 1.0×10^{-5} eV. In addition, a correction based on the Hubbard U model was used for the d orbitals of Ti atoms to obtain more accurate correlation energy, and the U value was 3.4 eV. For the slab model[5], the vacuum layer with a thickness of 15 Å was established to avoid layer-to-layer interaction.

The data obtained by XRD were imported into Origin software, and then the diffraction peak 2θ values of (121) (040) (042) were obtained by Lorentz fit. Brag Equation (1) was used to obtain the plane spacing, and the Williamson-Hall (W-H) Equation (2) was used to calculate the strain.

$$d = \frac{n\lambda}{2sin\theta} \quad (1)$$

Where n =1, λ =1.5406 Å.

$$\beta cos\theta = \frac{k\lambda}{D} + 4sin\theta \quad (2)$$

Where β is symbolized for the full width at half maxima (FWHM). k = 0.9, λ =1.5406 Å.

Geometric Phase Analysis (GPA) on HRTEM images used the GMS plug-in FRWR tools

2. Supplementary Figures

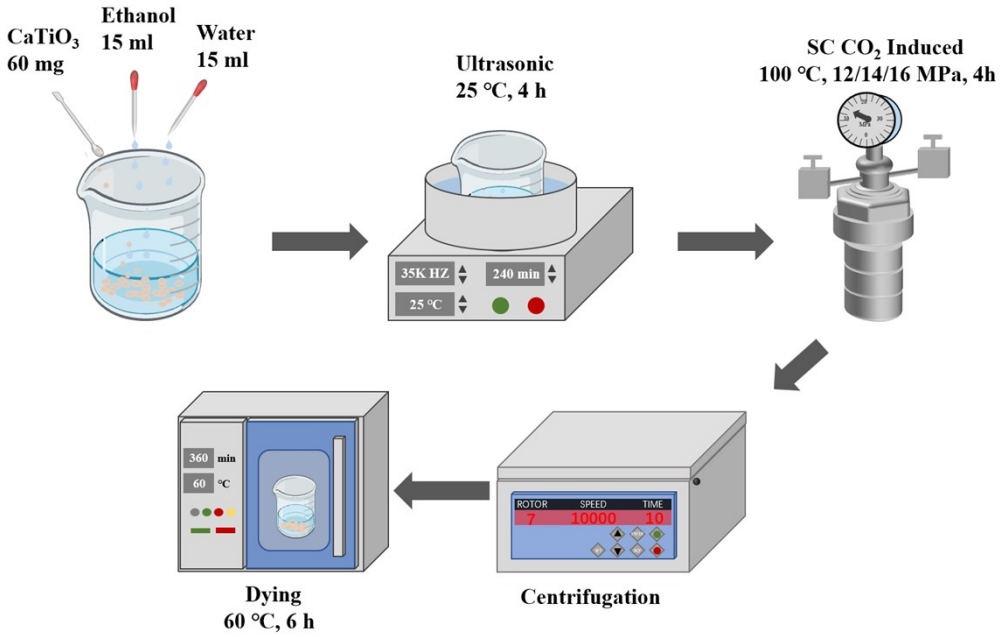

Supplementary Fig. 1| Experimental flow chart of $CaTiO_3$ preparation in this work.

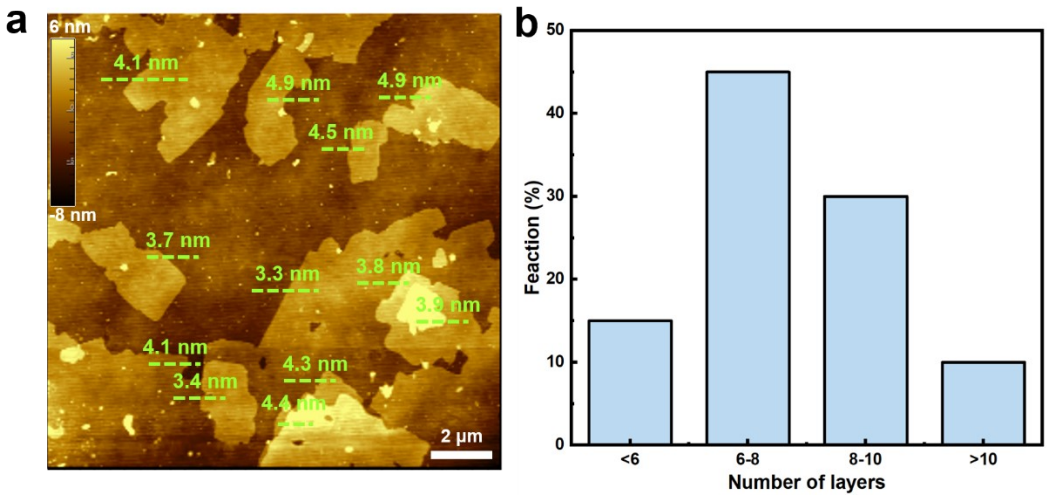

Supplementary Fig. 2| AFM of $CaTiO_3$ processed by SC CO_2 under 16 MPa. a, AFM image. inset: sample thickness diagram of the white line in (a). b, Thickness distribution diagram of (a).

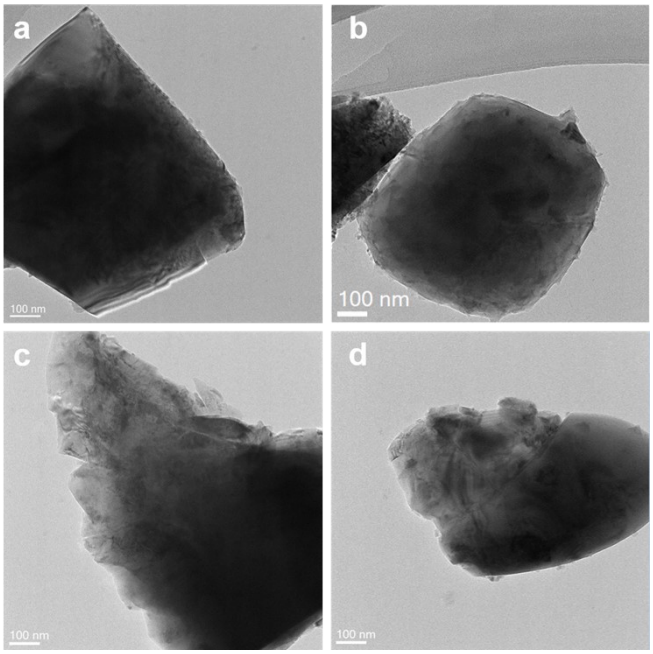

Supplementary Fig. 3| Low-magnification TEM images of $CaTiO_3$ samples under different experimental conditions. a, ultrasonic treatment. **b-d,** SC CO_2 under different pressures, the pressure sequence corresponding to b-d is 12, 14 and 16MPa.

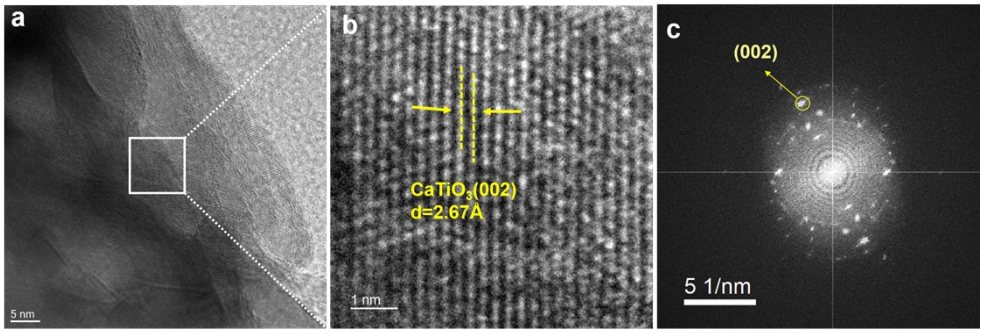

Supplementary Fig. 4| Experimentally presentation of atomic arrangement of $CaTiO_3$ processed by ultrasonic. a, HRTEM images. **b,** HRTEM images of the region enclosed by the white square in (a).**c,** FFT patterns of the region enclosed by the white squares in (a).

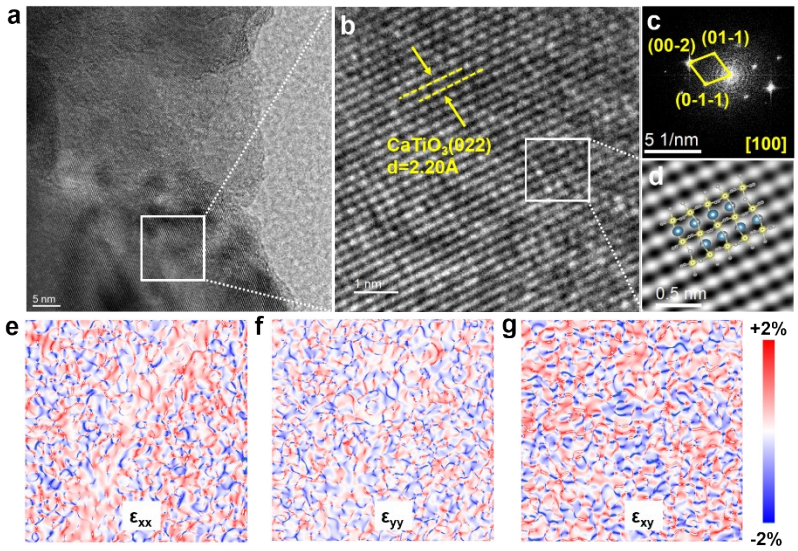

Supplementary Fig. 5| Experimentally presentation of atomic arrangement of $CaTiO_3$ processed by SC CO_2 under 12 MPa. a, HRTEM images. **b,** HRTEM images of the region enclosed by the white square in (a). **c,** FFT patterns of the region enclosed by the white squares in (a). **d,** Filtered images of the HRTEM images of the region enclosed by the white square in (b). **e,** Geometric Phase Analysis (GPA) along the x-axis direction. **f,** GPA along the y-axis direction. **g,** The corresponding strain map of shear strain ε_{xy}.

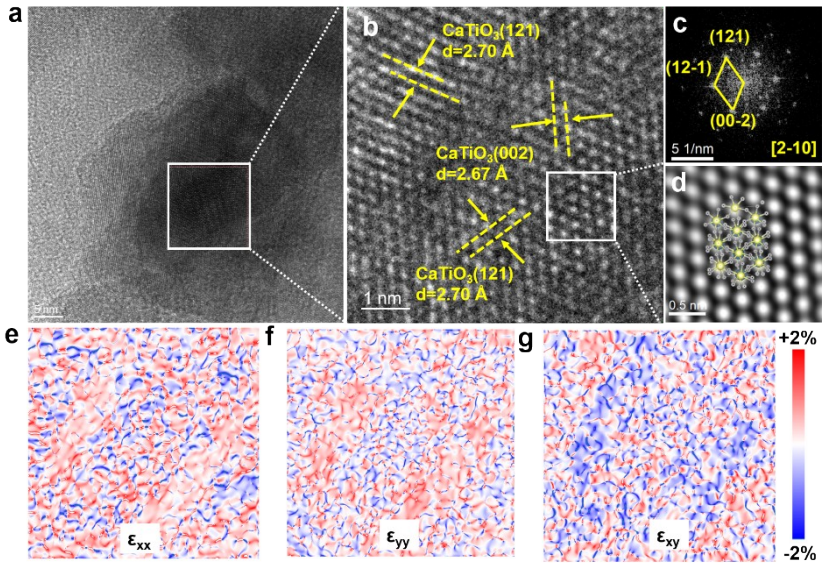

Supplementary Fig. 6| Experimentally presentation of atomic arrangement of $CaTiO_3$ processed by SC CO_2 under 14 MPa. a, HRTEM images. **b,** HRTEM images of the region enclosed by the white square in (a). **c,** FFT patterns of the region enclosed by the white squares in (a). **d,** Filtered images of the HRTEM images of the region enclosed by the white square in (b). **e,** Geometric Phase Analysis (GPA) along the x-axis direction. **f,** GPA along the y-axis direction. **g,** The corresponding strain map of shear strain ε_{xy}.

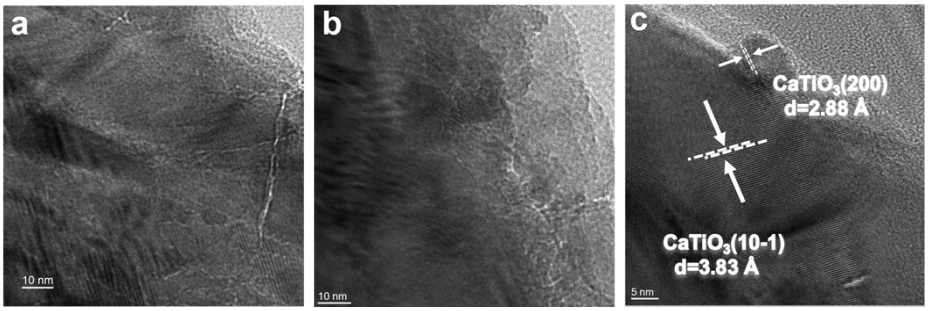

Supplementary Fig. 7| HRTEM image of 16 MPa $SCCO_2$-treated $CaTiO_3$.

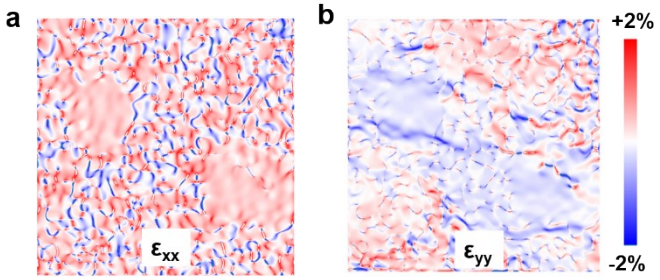

Supplementary Fig. 8| GPA of $CaTiO_3$ sample under 16 MPa pressure treatment. **a,** Along the y-axis direction. **b,** The corresponding strain map of shear strain ε_{xy}.

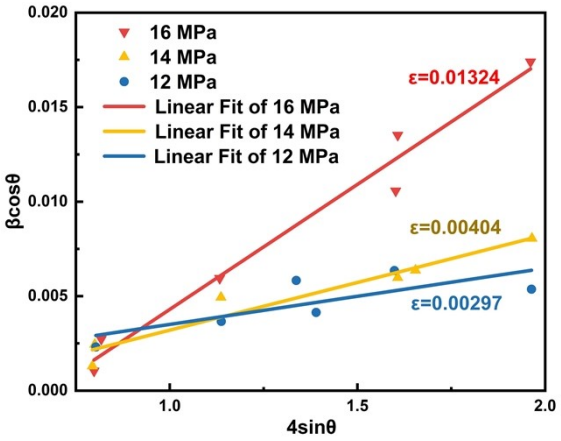

Supplementary Fig. 9| The W-H plot for strain in $CaTiO_3$ crystal structure. The values of slopes of linear equation have been used to determine the micro-strain of sample.

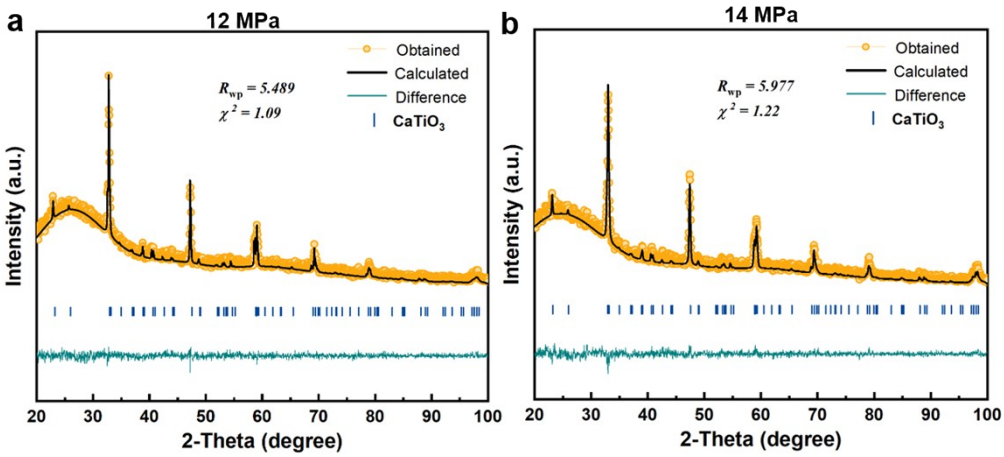

Supplementary Fig. 10| The Rietveld-refined XRD patterns of $CaTiO_3$ under different pressure of CO2. a, 12MPa. **b,** 14MPa.

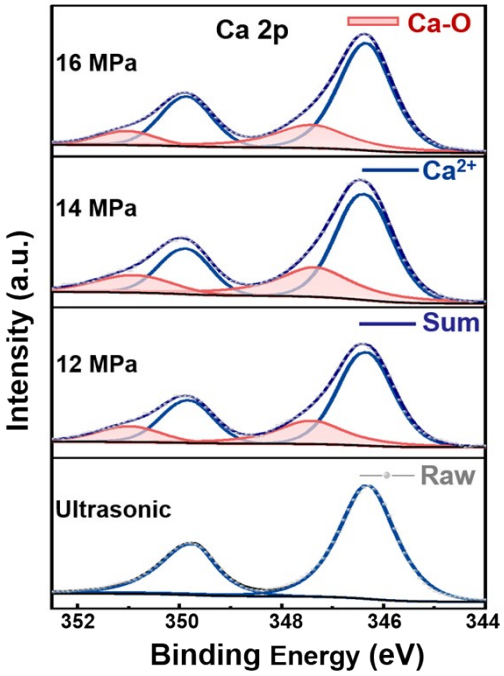

Supplementary Fig. 11| The Ca 2p XPS characterization of $CaTiO_3$ samples under different pressure treatments.

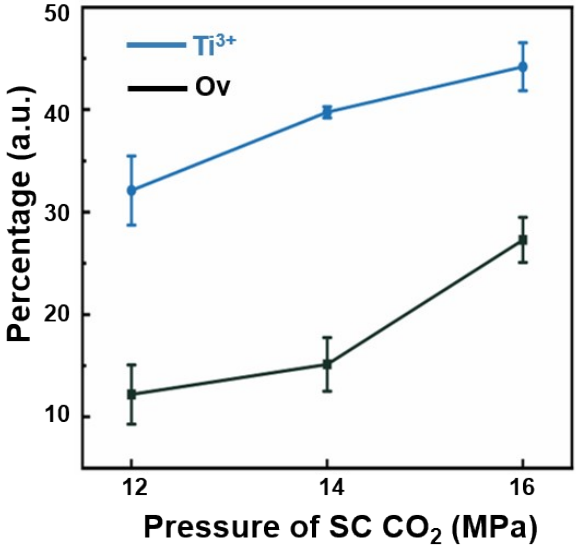

Supplementary Fig. 12| Variation of the Ti^{3+} and O_v with increasing SC CO_2 pressure.

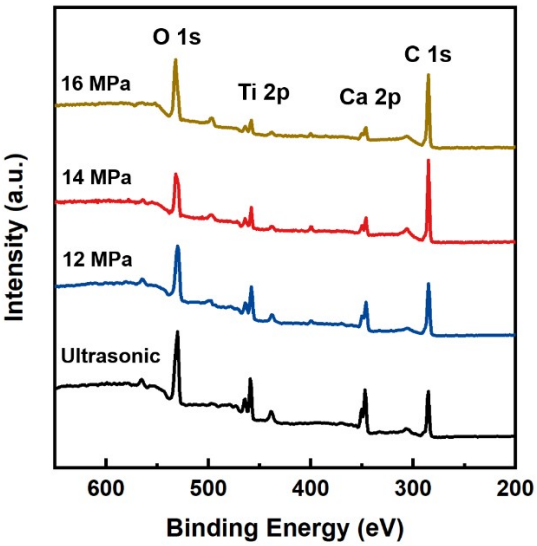

Supplementary Fig. 13| XPS Survey characterization of $CaTiO_3$ samples under different pressure treatments, and there is no other impurity element in the sample.

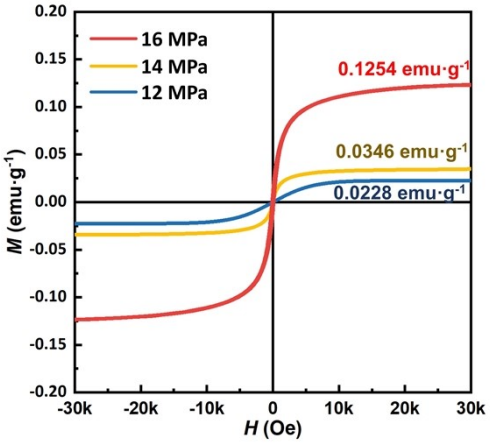

Supplementary Fig. 14| M-H curve of $CaTiO_3$ samples under the same conditions

3. Supplementary Tables

Supplementary Table 1| The lattice spacing and stretching ratio under different pressure of SC CO_2

Plane	Pressure (MPa)	D (nm)	Δd (nm)	Strain %
(101)	standard	3.8240	-	-
	12	3.8364	0.0123	0.3237
	14	3.8495	0.0255	0.6657
	16	3.8826	0.0586	1.5313
(121)	standard	2.7010	-	-
	12	2.7073	0.0063	0.2347
	14	2.7105	0.0095	0.3524
	16	2.7298	0.0288	1.0649
(040)	standard	1.9110	-	-
	12	1.9125	0.0015	0.0776
	14	1.9155	0.0045	0.2363
	16	1.9216	0.0106	0.5552
(042)	standard	1.5570	-	-
	12	1.5578	0.0007	0.0473
	14	1.5597	0.0027	0.1689
	16	1.5635	0.0065	0.4132

Supplementary Table 2| The parameters for fitting the lattice structure of $CaTiO_3$ under different pressure treatments.

Pressure (MPa)	Lattice parameters a (Å)	Lattice parameters b (Å)	Lattice parameters c (Å)	Vol ($Å^3$)	Average bond length (Å)		Distortion index (bond length)
					Ti-O_1	Ti-O_2	
Standard	5.4405	7.6436	5.3812	223.77	1.9508	9.9637	0.0015
12	5.4438	7.6442	5.3832	224.01	1.9507	9.9746	0.0017
14	5.4451	7.6442	5.3832	224.07	1.9510	9.9766	0.0017
16	5.4453	7.6450	5.3831	224.10	1.9516	9.9784	0.0017

Supplementary Table 3. The Ms, Mr and Hc value under different pressure of CO2.

Pressure (MPa)	Ms×10^{-2} (emu·g^{-1})	Mr×10^{-2} (emu·g^{-1})	*Hc (Oe)*
12	2.29	0.23	55.51
14	6.03	0.39	59.92
16	16.61	1.17	71.44

4. References

1. G. Kresse and J. Furthmüller, *Computational Materials Science*, 1996, **6**, 15-50.
2. G. Kresse and D. Joubert, *Phys. Rev. B.*, 1999, **59**, 1758-1775.
3. J. P. Perdew, K. Burke and M. Ernzerhof, *Phys. Rev. Lett.*, 1997, **78**, 1396-1396.
4. S. Grimme, S. Ehrlich and L. Goerigk, *J. Comput. Chem.*, 2011, **32**, 1456-1465.
5. H. J. Monkhorst and J. D. Pack, *Phys. Rev. B.*, 1976, **13**, 5188-5192.